Neuromorphic meets neuromechanics, part I: the methodology and implementation

2017 J. Neural Eng. 14 025001

(http://iopscience.iop.org/1741-2552/14/2/025001)

IOP Publishing Journal of Neural Engineering
J. Neural Eng. **14** (2017) 025001 (12pp) doi:10.1088/1741-2552/aa593c

Neuromorphic meets neuromechanics, part I: the methodology and implementation

Chuanxin M Niu[1,2], Kian Jalaleddini[3], Won Joon Sohn[3], John Rocamora[4], Terence D Sanger[3,4,5,6] and Francisco J Valero-Cuevas[3,4,6,7]

[1] Department of Rehabilitation Medicine, Ruijin Hospital, School of Medicine, Shanghai Jiao Tong University, Shanghai, People's Republic of China
[2] Med-X Research Institute, School of Biomedical Engineering, Shanghai Jiao Tong University, Shanghai, People's Republic of China
[3] Division of Biokinesiology and Physical Therapy, 1042 Downey Way, Los Angeles, CA 90089, United States of America
[4] Department of Biomedical Engineering, 1042 Downey Way, Los Angeles, CA 90089, United States of America
[5] Neurology, University of Southern California, 1042 Downey Way, Los Angeles, CA 90089, United States of America

E-mail: valero@usc.edu

Received 7 August 2016, revised 29 November 2016
Accepted for publication 13 January 2017
Published 13 February 2017

Abstract

Objective: One goal of neuromorphic engineering is to create 'realistic' robotic systems that interact with the physical world by adopting neuromechanical principles from biology. Critical to this is the methodology to implement the spinal circuitry responsible for the behavior of afferented muscles. At its core, muscle afferentation is the closed-loop behavior arising from the interactions among populations of muscle spindle afferents, alpha and gamma motoneurons, and muscle fibers to enable useful behaviors. *Approach*. We used programmable very-large-scale-circuit (VLSI) hardware to implement simple models of spiking neurons, skeletal muscles, muscle spindle proprioceptors, alpha-motoneuron recruitment, gamma motoneuron control of spindle sensitivity, and the monosynaptic circuitry connecting them. This multi-scale system of populations of spiking neurons emulated the physiological properties of a pair of antagonistic afferented mammalian muscles (each simulated by 1024 alpha- and gamma-motoneurones) acting on a joint via long tendons. *Main results*. This integrated system was able to maintain a joint angle, and reproduced stretch reflex responses even when driving the nonlinear biomechanics of an actual cadaveric finger. Moreover, this system allowed us to explore numerous values and combinations of gamma-static and gamma-dynamic gains when driving a robotic finger, some of which replicated some human pathological conditions. Lastly, we explored the behavioral consequences of adopting three alternative models of isometric muscle force production. We found that the dynamic responses to rate-coded spike trains produce force ramps that can be very sensitive to tendon elasticity, especially at high force output. *Significance*. Our methodology produced, to our knowledge, the first example of an autonomous, multi-scale, neuromorphic, neuromechanical system capable of creating realistic reflex behavior in cadaveric fingers. This research platform allows us to explore the mechanisms behind healthy and pathological sensorimotor function in the physical world by building them from first principles, and it is a precursor to neuromorphic robotic systems.

Keywords: reflex, modeling, neuromorphic engineering, neuromuscular control, neuromechanics

(Some figures may appear in colour only in the online journal)

[6] Equal leadership.
[7] Author to whom any correspondence should be addressed.

Introduction

Which minimal features of the human sensorimotor nervous system are the *sine qua non* for healthy function in the physical world? And, how do these features lead to pathology or provide opportunities for treatment? Neuroanatomists and electrophysiologists since the time of Sherrington have mapped the circuitry in the human spinal cord. But it is still unclear how the known spinally-mediated neural mechanisms can naturally and robustly contribute to healthy voluntary function and to clinical symptomatology such as flaccidity, tremor, and spasticity. There is no animal model for the human spinal neural system given its known evolutionary adaptations—especially for the human hand [1–3]. Moreover, it is difficult and invasive to use microneurography to quantify the dynamical interactions among upper and lower motoneurones, proprioceptors, muscles, and tendons in humans. Today's dominant reductive approach to understanding of human sensorimotor function will continue to have these limitations even after collecting massive amounts of additional *in vivo* neural recordings.

A promising alternative is to create a synthetic (in the integrative sense) and physiologically realistic system to identify what types of neural interaction are necessary and sufficient to reproduce the observed human healthy and pathologic behavior—and putting it to the ultimate test of physical implementation. The history of such a synthetic analysis approach for information processing in neuroscience dates back to the 1940s, when scientists started creating artificial neurons and neural networks using analog electronic circuits [4]. Dynamic models of neurons on digital computers soon followed [5, 6]. Special-purpose hardware acceleration using very large scale integrated-circuit (VLSI) technology started to provide some key insights in neural computation, including asynchrony among neurons, spike representation of information, and self-improving mechanisms such as plasticity [7–10]. This so-called 'neuromorphic' hardware has been successfully applied to understanding mechanisms of memory [11], visual representation [12], and recently cognitive function [13].

It remains challenging to use this synthetic approach for understanding sensorimotor function given the many complex and often nonlinear subsystems involved. For example, a model of even the monosynaptic stretch-reflex is likely to be inadequate unless it contains all of the following: a population of neurons (sensory and motor); the peripheral physiological elements (muscles, proprioceptors, skeletal system) with which those neurons interact [14]; the nonlinear viscoelastic and biomechanical system moved by the muscles; and the physical environment with which the full system must interact. The computational cost of spike-to-spike simulation usually slows the entire system down, thus making it difficult to couple such a non-real-time system with real objects interacting in the physical world.

This paper presents what to our knowledge is the first autonomous, multi-scale, physiologically faithful neuromorphic system to implement the neuromechanical features of afferented muscles in real-time from neurons to physical finger function. Our methodology is critically enabled by our recently developed VLSI neuromorphic platform [15] and a new design of the actuators of the neuromechanical plant. This synthetic analysis approach creates sensorimotor circuits that are biologically realistic but emulated on non-biological hardware.

We demonstrate the exploration of the functional significance of spinal proprioceptive monosynaptic pathways, their afferent gains, and their dynamical interaction with a cadaveric finger's actual skeletal structures and functions. In principle, the monosynaptic spinal pathways can provide fast, continuous feedback control that presumably has a stabilizing effect on human joints. However, it is not clear which structures and features are essential for joint stabilization. To this purpose, testing a minimal sensorimotor system is a critical first step. Furthermore, we consider the cadaver experiment the most rigorous test to date of a physical neuromorphic sensorimotor model, since it includes the actual nonlinearities of anatomical tissues and the biomechanics of a real joint—which is the very challenge confronting a biological sensorimotor nervous system. It is non-trivial for a closed-loop system—which has nonlinear sensory input, nonlinear motor output, noisy signal transduction, and prominent conduction delays—to achieve simple tasks such as maintaining a static posture in the presence of perturbation.

Our neuromorphic implementation of a sensorimotor system follows a systematic build-up from pure software simulation, to a scalable VLSI hardware design, to a hardware-in-the-loop robotic joint, and finally a neuromorphically controlled human cadaver. We consider each phase essential for validating technical soundness and physiological realism. Our eventual goal is to validate or revise our understanding of the neuromechanical mechanisms at the foundation of sensorimotor function. If successful, this work will allow for a new paradigm for systematic understanding of sensorimotor health, disease and treatment.

Methods

System architecture

The emulated sensorimotor system consisted of an antagonist pair of muscles each with a non-reciprocal stretch reflex, including the muscle spindles, spindle afferents, and alpha-motoneuron pools of the simulated *extensor indicis proprius* and *flexor digitorum profundus* muscles (figure 1). Briefly, the following events occur when establishing tensions in an emulated muscle: (1) a train of alpha-motoneuron spikes activates a muscle model; (2) the muscle model computes the current muscle force, based on physiological activation-contraction dynamics and force-length and force-velocity properties of skeletal muscle; (3) the current muscle force is generated by brushless DC motors controlled in real-time as a torque follower; (4) the ensuing changes in muscle length and velocity are transduced and sent to emulated muscle spindles, thus incurring subsequent reflex behavior. See figure 1(C) for the final design of the system.

For each of the two muscles, all spiking neuron behavior was generated autonomously and in real-time by a low-cost FPGA

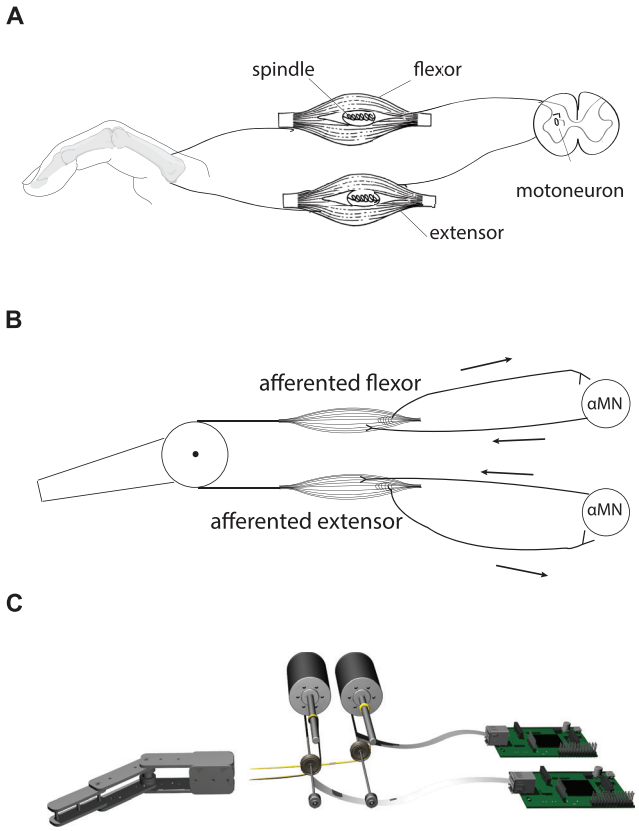

Figure 1. (A) Components of the human sensorimotor system focused on in this study. The system includes a finger joint comprising two opposing monoarticular muscles (abductor and adductor), muscle spindles, spindle afference, and alpha-motoneuronpools. (B) Model of the neuromuscular system in this study. Our model includes monosynaptic connections with 32 ms loop-delay. (B) Conceptualized block diagrams. (C) Final design of the system with an illustration of the robotic joint, muscle simulated using DC torque motor; spinal cord simulated using neuromorphic hardware based on FPGA.

(Xilinx Spartan-6). It emulated 256 spindle afferents [16, 17], 1024 spiking neurons (768 alpha-motoneurones plus 256 sensory neurons = 1024) as simplified by Izhikevich [16, 18], and a lumped-parameter muscle model in parallel with a model of the associated surface electromyogram (EMG). This setup had multiple parallel proprioceptive closed-loop pathways, resembling the concurrent monosynaptic pathways in human spinal cord [19]. The hardware emulates parallel proprioceptive pathways including monosynaptic connections with 32 ms loop-delay representing the spinal proprioceptive pathway. The delays were chosen to approximate known conduction delays.

For each muscle, the 768 alpha-motoneurons were divided into 6 groups representing motor units of 6 different sizes (figure 2(A)). This allowed us to implement a system in which Henneman's size principle [20] emerged naturally during simulated voluntary motor unit recruitment. In one experiment (See *Results*, NEURONAL BEHAVIOR), we emulated 20 groups of motor units to better demonstrate their recruitment order; in the rest of experiments we reduced to number of motor units to 6 due to computational cost. The neuromorphic system was also connected to a fresh-frozen, unfixed, cadaveric hand specimen—where the two muscles drove the metacarpophalangeal joint of the cadaver index finger by pulling on the tendons of the *extensor digitorum communis* and *flexor digitorum profundus* (figure 2(B)). The mathematical definitions of the components corresponding to figure 2(A) are listed in table 1. Our only algorithmic constraints in the platform were that the adjacent components must have compatible interfaces, and the interfacing variables must also be physiologically attainable. The behavior of the system emerges from the interaction of emulated components.

Neuron

We used Izhikevich's simplification [16] of the classic Hodgkin–Huxley model [5] for neuron emulation. The Izhikevich model takes the postsynaptic neural current as the input and produces a spike train as the output. We chose the Izhikevich model for the combination of accurate approximation to spiking dynamics and computational efficiency. Neuronal synapses were implemented using a simple model based on neural recording of hair cells in rats [21], which characterized the rising time and falling time profile of the EPSC (excitatory post-synaptic current) as follows:

$$I(t) = \begin{cases} V_m \times \left(e^{-\frac{t}{\tau_d V_m}} - e^{-\frac{t}{\tau_r V_m}} \right) & \text{if } t \geqslant 0 \\ 0 & \text{otherwise} \end{cases}$$

The key parameters in this synapse model are the time constants for rise (τ_r) and decay (τ_d) of the postsynaptic potential. In our emulation $\tau_r = 0.001$ s and $\tau_d = 0.003$ s. Our approach of neuron emulation has been previously reported [18].

Muscle

Muscle converts individual motor unit action potentials (MUAPs) to force. The time course of a twitch is sluggish compared to MUAPs as a result of the release, diffusion and reuptake of calcium by the sarcoplasmic reticulum [22, 23] as well as the effects of connective tissue viscoelasticity on cross-bridge dynamics [24]. Moreover, the resulting muscle force changes according to its length and velocity (as per the force-length and force-velocity properties), and history of its active state [25]. All these dynamics are muscle fiber-type dependent [26]. Consequently, a muscle model critically implements the dynamic relationship that gives rise to its force as functions of the action potential firing rate, muscle type, instantaneous length, and shortening velocity.

Three alternative muscle models were implemented and compared according to their responses to neuromorphic MUAPs. The first muscle model is a linear, second-order, low-pass filter. The impulse response of a low-pass filter naturally and credibly characterizes the muscle force elicited by each motoneuron spike (a muscle twitch) [19]. This simplest of dynamical models allows the width of a muscle twitch to be easily adjusted. We enforced the low-pass filter to be critically-damped, therefore the oscillations common in second-order systems were eliminated to forbid negative forces that are unrealistic for muscles. The free parameters,

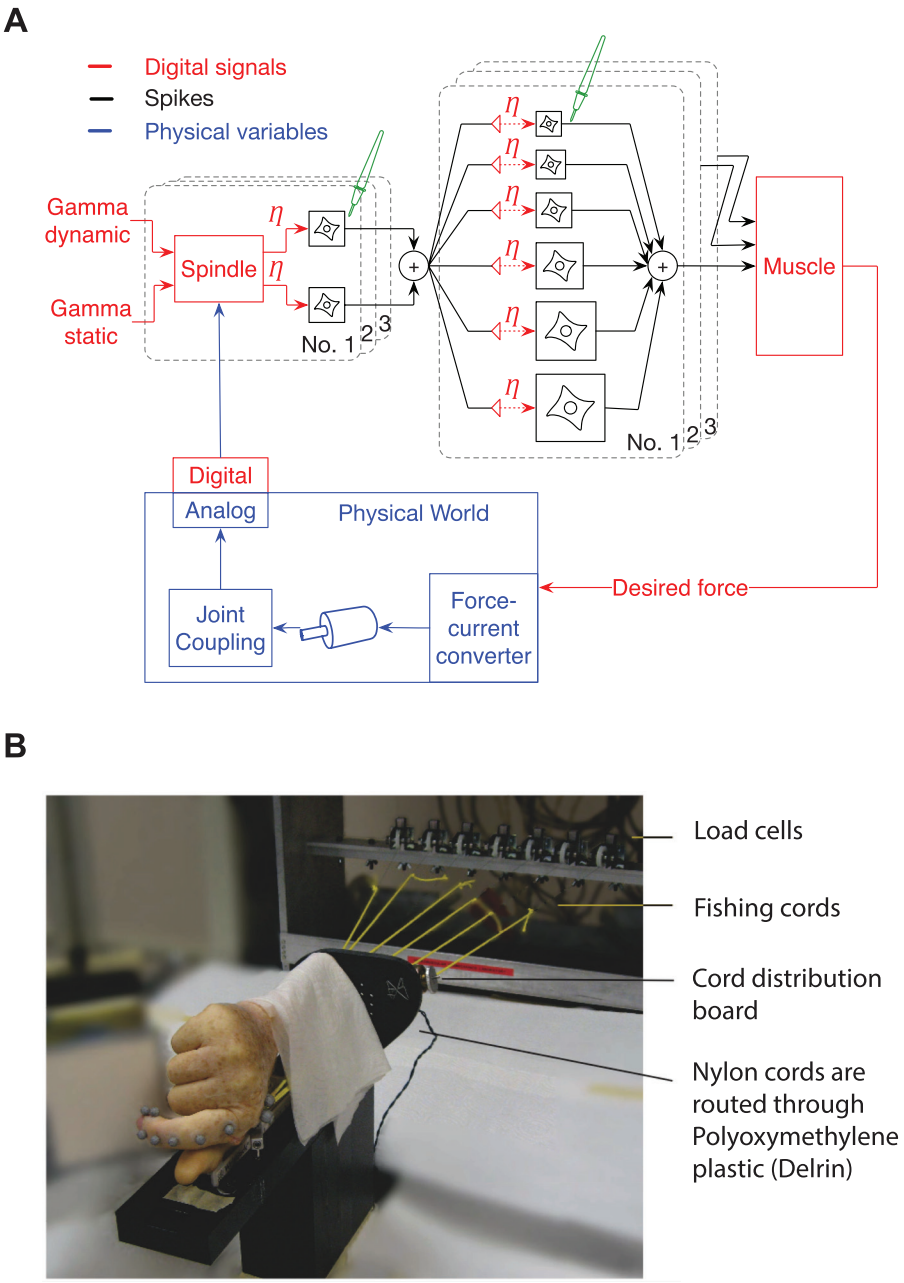

Figure 2. (A) Detailed implementation of the motor nervous system on neuromorphic hardware. The components are implemented separately for the flexor and extensor, which simultaneously drive the joint modeled as a beam freely rotating around the endpoint. For each muscle, the muscle force is calculated from a muscle model activated by 6 motoneuron pools of different sizes, each pool comprising of 128 motoneurons modeled by Izhikevich [16]. The motoneuron pools receive excitatory input from the spinal loop. In the spinal loop, the sensory feedback is provided by muscle spindles implemented as Mileusnic and colleagues did [17], which include both the Primary (Ia) and Secondary (II) afferences to provide the dynamic and static proprioceptive information about the muscle. A total of 128 spindles are implemented for each muscle, thus providing 128 spiking afferents. Due to the limited capacity of each FPGA unit, the system must be distributed on multiple FPGAs. The entire system uses 4 FPGA boards enabling 2 muscles with 2300 neurons. Only half of the system (abductor) is shown. (B) The cadaver finger setup that provides realistic joint configuration and tendon elasticity for the neuromorphic system to activate. In this study, only the metacarpophalangeal joint of the index finger was involved.

e.g. gain, damping ratio and natural frequency of the filter had been estimated from an isometric force generation task in the absence of fatigue [22]:

$$\frac{F(s)}{I(s)} = \frac{62\,178.5}{s^2 + 62.8s + 987.0}$$

where $F(s)$ is muscle force, $I(s)$ is the neural spike train, and s indicates the Laplace transform.

The second muscle model is an accepted version of the well-known Hill-type model [27]. The Hill-type model uses standalone mechanical components to approximate features during muscle contraction, e.g. force production, viscoelasticity, sudden release, etc. Our implementation was identical to that described in Shadmehr and Wise [28] with an interface to receive and integrate real-time spiking MUAPs. The active force generation component of the model in the isometric condition was:

$$\frac{F(s)}{A(s)} = \frac{1.33}{0.49s + 2.1}$$

$$\frac{A(s)}{I(s)} = \frac{48144}{s + 30.6} - \frac{45845}{s + 29.4}$$

where $A(s)$ is the muscle activation.

The third muscle model is the two-element Hill-type model that differentiates fast and slow muscle fibers. This model includes a series of nested first order differential equations with time-varying dynamics to generate the muscle active state. The structure of the model followed Wakeling *et al* [29]. The active force generation component of the model in the isometric condition was:

$$\frac{\mathrm{d}}{\mathrm{d}t}a_1(t) + [1/\tau_1(\beta_1 + [1 - \beta_1]\, i(t))]\, a_1(t) = \frac{i(t)}{\tau_1}$$

$$\frac{\mathrm{d}}{\mathrm{d}t}a_2(t) + [1/\tau_1(\beta_2 + [1 - \beta_2]\, a_1(t))]\, a_2(t) = \frac{a_1(t)}{\tau_2}$$

$$\frac{\mathrm{d}}{\mathrm{d}t}F_{\mathrm{type}}(t) + [1/\tau_1(\beta_3 + [1 - \beta_3]\, a_2(t))]\, F_{\mathrm{type}}(t) = c\frac{a_2(t)}{\tau_3}$$

$$F(t) = F_{\mathrm{slow}}(t) + F_{\mathrm{fast}}(t)$$

where $\{\beta_1, \beta_2, \beta_3, \tau_1\, \tau_2\, \tau_3\}$ was $\{0.73, 0.74, 0.92, 34.06, 36.27, 37.82\}$ for slow muscle fibers and $\{0.90,\ 0.99,\ 0.98,\ 18.14,\ 20.91,\ 20.75\}$ for fast muscle fibers.

Muscle spindle

Each muscle was assigned 128 muscle spindles following a lumped-parameter spindle model characterizing cat soleus spindles [17]. We know of no model for human muscle spindles that is as well validated. This model requires static and dynamic gamma-motoneuron inputs represented as sensor gains to tune the pattern of afferent spike trains. Our neuromorphic implementation of muscle spindle and its spiking afferents followed Mileusnic *et al* [15].

Motor unit pool

As mentioned above, for each muscle, 768 alpha-motoneurons were divided into 6 groups representing motor units of 6 various sizes. As a result, Henneman's size principle emerged naturally during the hardware-in-the-loop emulation for voluntary motor unit recruitment (figure 3(A)), our emulated results were qualitatively similar to the motoneuron activities decomposed from human EMG [30]. Each size of motor unit was emulated with 128 stochastic copies, i.e. noise was added to each copy such that all 128 motor units fire at random even when their inputs are identical. Pseudorandom white uniform noise (5 mV amplitude) was added to the membrane potential of each neuron to emulate the large number of inputs that a neuron usually receives from the dendritic tree. The noise level was set to create a typical 4.8 mV fluctuation in the membrane potential [31]. Pseudorandom noise is generated using a linear-feedback-shift-register [32].

Table 1. The mathematical definitions of the components for the neuromorphic implementation of sensorimotor system.

Component	Mathematical definition
Neuron	$S^*_{\mathrm{neuron}}(t) = f_{\mathrm{neuron}}(I, t)$
Synapse	$I(t) = f_{\mathrm{synapse}}(S^*, t)$
Spindle	$S^*_{\mathrm{afferent}}(t) = f_{\mathrm{spindle}}(L, \dot{L}, \Gamma_{\mathrm{dynamic}}, \Gamma_{\mathrm{static}}, I, t)$
Muscle	$T(t) = f_{\mathrm{muscle}}(S, L, \dot{L}, t)$
Joint	$F(t) = f_{\mathrm{muscle}}(T, t)$

* = Spiking signal.

The size of a motor unit was not explicitly modeled. We focused on the effect that small motor units require less EPSP to activate due to lower capacitance and membrane resistance; therefore, we implemented the size of a motor unit by changing the excitability of the motoneuron and the resulting twitch force. Details on motor unit emulation were previous reported [18].

Mechanical Embodiment of an agonist-antagonist muscle pair driving a single planar joint: Robotic finger

The implementation shown in figure 1(C) is a robotic mechanical finger with one joint, with the distal joint splinted to allow rotation only at the proximal joint. The total length of the finger from the axis of rotation to the tip of the finger was 12.5 cm. The joint had a movement range of 120°, with a moment of inertia of approximately 2.63×10^{-4} kg m^{-2} (a total mass of 0.049 kg). Tendons were attached to the joint through a pulley of 8.8 mm in radius. The pulley was attached to the distal segment of the joint, such that any tension in the tendon resulted in a torque applied to the distal segment. Kevlar strings (Model 8800K41) were used as surrogates of muscle tendons. Each tendon was wrapped around the axle of its motor (see below) to generate tension in it, and incremental encoders (model HEDS-5500, Avago Technologies) mounted on the motor axle transduced tendon excursion in real-time.

The desired musculotendon force was computed from the muscle models in real-time with 1 kHz sampling rate. That digital force signal was then transformed into an analog force signal using a NI PXI-6723 D/A card (13 bits resolution), which was used as the reference signal to control the force of a Faulhaber DC motor (model 3863h024c). The motor driver was an LDUS1 (Western Design) with PCU-S3 Chassis. The low-level control law was a PID controller optimized using MATLAB Control System Toolbox for our DC motor that had a bandwidth of 34.5 Hz, above which the driving signals would be attenuated by the DC motor itself. The tendon force was measured by a load cell (Interface SML 10) holding a pulley that guides the Kevlar tendon. A signal conditioner (Interface model SGA) amplified the output of the load cell. The force was converted to digital using a NI PXI-6250 D/A card and sampled at 1 kHz for the low level controller and acquisition purposes.

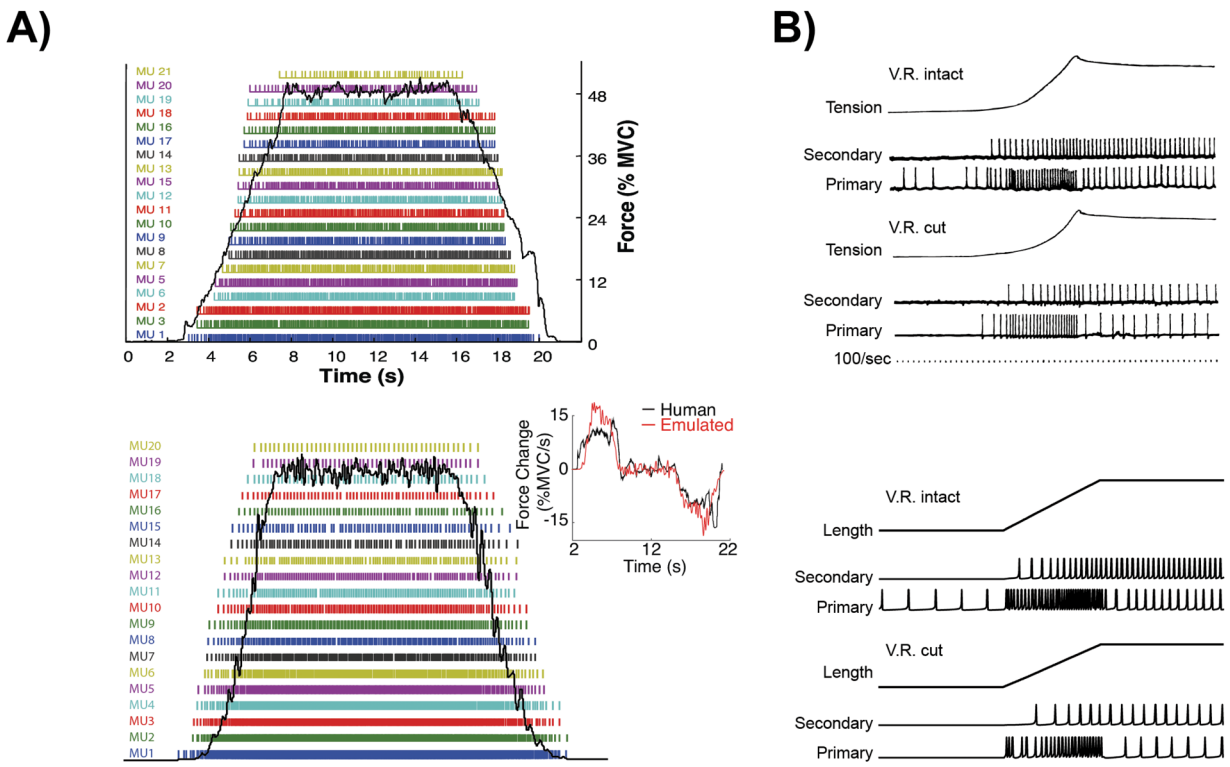

Figure 3. (A) The spiking behavior of motoneuron from human data [35] (upper panel, reproduced with permission) and our emulation (lower panel). The emulation included 20 motor units with different sizes to verify Henneman's sizeprinciple. As expected, the emulated motor units show a progressive recruitment order that is qualitatively similar to human data. The inset compares the force change pattern between human (black) and emulation (red). (B) Similar to cat soleus spindles [36] (upper panel, reproduced with permission), the action potential of spindle afferents from FPGA emulation (lower panel) show distinguishable patterns between Primary and Secondary fibers. The differentiation between ventral root intact and ventral root cut was also compatible, i.e. the firing rate reduced without ventral root input.

Mechanical embodiment of an agonist-antagonist muscle pair driving a single planar joint: Cadaver finger

A critical test of our implementation is to control a real biomechanical plant in the form of a cadaver finger that is not chemically preserved. As in prior studies [33], we actuated the tendons of a cadaveric index finger with electric motors. This involved thawing a fresh frozen cadaver arm, resecting it at the mid-forearm level, and removing all muscle, skin and fat tissue to dissect and isolate the proximal end of the insertion tendons of the muscles of interest. In this study, only the insertion tendons of the *flexor digitorum profundus* and *extensor indicis proprius* were dissected and isolated. We fixed the specimen rigidly to a tabletop using an external fixator (Agee-WristJack, Hand Biomechanics Lab, Inc., Sacramento, CA), and tied and glued (Vetbond, 3M, St Paul, MN) the proximal end of the tendons to Kevlar cords attached to our brushless DC motors.

Electromyography (EMG)

Another measurable output of muscle is its EMG. We implemented a surface EMG model by superimposing MUAPs from 6 sizes of motor unit pools, with each MUAP modeled as a bipolar waveform approximated by two cascaded exponential filters. This produced realistic surface EMG signals as described in previous studies [34].

Experiments: muscle function, muscle spindle function, and emergent closed-loop stretch reflex

We systematically implemented and validated the functional features of the neuromorphic system at three functional levels: muscle function, muscle spindle function, and emergent closed loop stretch reflex. Table 2 shows the functional features tested at four complexity levels of implementation: software simulation (MATLAB Simulink, Mathworks Inc.), hardware emulation (FPGA, Xilinx Inc.), robotic finger control, and cadaver finger control. Our implementations progressively approximated *in vivo* human sensorimotor function for monosynaptic stretch reflexes.

We verified the emulated multi-scale system in a series of experiments. First, the activity of motoneurons and spindle afferents was verified by comparing the emulated firing patterns to classic experimental results. Subsequently, muscle functions were verified when producing twitch response and unfused and fused tetanus responses. The stretch reflex, as the primary emergent behavior, was verified by applying mechanical force perturbations to the robotic finger. We created force perturbations using a Phantom Desktop haptic robot (Phantom Premium 1.0, Sensable Group) that applied a 4.0 N horizontal force pulse perturbation lasting 20 ms. We also created position perturbations using a servomotor (Dynamixel RX-28) rotating the joint by approximately 30° for at least 1 s. Lastly, we verified the closed-loop behavior of gamma-dynamic and

Table 2. The systematic progression for the neuromorphic implementation of sensorimotor system.

	Motoneuron size-principle (figure 3)	Spindle afferents (figure 3)	Muscle properties (figure 5)	Monosynaptic reflex (figure 6)	Disambiguate gamma static versus dynamic (figure 4)
Software simulation	○	○	○	○	○
Hardware emulation	♦	♦	♦	○	○
Robotic finger				♦	○
Cadaveric finger					♦

♦ = Shown in this report.
○ = Implemented but not shown.

gamma-static input when driving a cadaveric finger. In all experiments we recorded all variables in figure 1(D).

Results

Neuronal behavior

Figure 3 shows the spiking behavior of motoneuron and spindle afferents. In this experiment, we emulated 20 motor units with different sizes to verify that Henneman's size-principle could be reproduced. As expected, the emulated motor units show a progressive recruitment order that is qualitatively similar to human data [30] (figure 3(A)).

The spiking behavior of spindle afferents was verified in a virtual stretch-and-hold experiment. Similar to the classic experiment on decerebrate cat, the muscle was stretched to 36.8% of its resting length, corresponding to the 14 mm elongation of cat soleus muscle [35]. Responses were recorded both in the presence (ventral roots intact) and absence (ventral roots cut) of tonic fusimotor activity. As can be seen in figure 3(B), the emulated Primary (Ia) afferent show stronger phasic response than Secondary (II) afferent; while the Secondary (II) afferent produced stronger tonic response. The results are qualitatively similar between biological and emulated experiments.

Gamma fusimotor drive behavior

We tested 4 combinations of gamma fusimotor drive (gamma dynamic low/high, gamma static low/high, low = 10 Hz, high = 200 Hz) to validate their relative contributions to the stretch reflex. A typical EMG response to a ramp-and-hold muscle stretch includes a burst and subsequent tonic components. We quantified the EMG burst as the average EMG amplitude between 20 ms and 220 ms after the onset of muscle stretch; while the subsequent 200 ms of averaged EMG was calculated to represent the tonic EMG response (representative traces are shown in figure 4(A)). The cadaver finger was stretched with 15 repetitions under each combination of gamma dynamic and static drive. Across repetitions, the EMG traces showed variability due to the synaptic noise implemented in our system. As expected, the EMG bursts were affected by both gamma dynamic and static drive, but dominated by gamma dynamic drive (figure 4(B)); the relative contributions of gamma dynamic and static drive were clearly disambiguated from EMG tonic responses (figure 4(C)).

Muscle behavior

Skeletal muscle has a low-pass response that converts alpha-motoneuron spikes into time-varying force twitches under temporal and spatial summation. The magnitude of the response depends on the muscle's instantaneous fiber length and shortening velocity. (We did not include a tendon of origin, since that would only have the effect of increasing the rise time of force and washing out the force-length properties [25].) In the cadaver finger, the tendon of insertion was the actual anatomical tendon. Our modular system allows the future implementation of any other muscle model by simply replacing it in the code that drives the DC motors. Future work will explore the consequences of implementing additional models as reviewed in [36, 37].

Figure 5 shows the software simulation and neuromorphic emulation of three muscle models when producing twitch response and unfused and fused tetanus responses. We systematically increased the action potential firing rate from 0.2 Hz to 80 Hz (figure 5(A)). In software simulation (figure 5(B)), the forces of the low-pass filter and simple Hill-type muscle models were almost identical. The two-element Hill-type model had a longer twitch contraction time. The twitch responses of the low-pass filter and Hill-type models started overlapping at 10 Hz whereas this happened at 5 Hz for the two-element model. The force became relatively constant (with individual twitches no longer perceptible) above 40 Hz for the two-element muscle and above 80 Hz for the others. Figure 5(C) demonstrates the forces measured from the robotic mechanical plant driven by our emulated system.

Reflex behavior

We tested the emergent behavior when the robotic finger with hardware-in-the-loop was perturbed by a second robot (Phantom Desktop, see Methods). Both gamma-dynamic and gamma-static drives were set to 80 Hz to provide moderate fusimotor activity. When perturbed using a ramp stretch (figure 6(A)), the multi-scale information shows that the force in the stretched muscle increased due to higher firing rates in the motoneuron pool (2 neurons from each of the 6 motor units are shown); the emulated EMG also confirms such reflex behavior. When perturbed using a 4.0 N (figure 6(B)), 20 ms force pulse, the robotic joint was displaced by ~30°

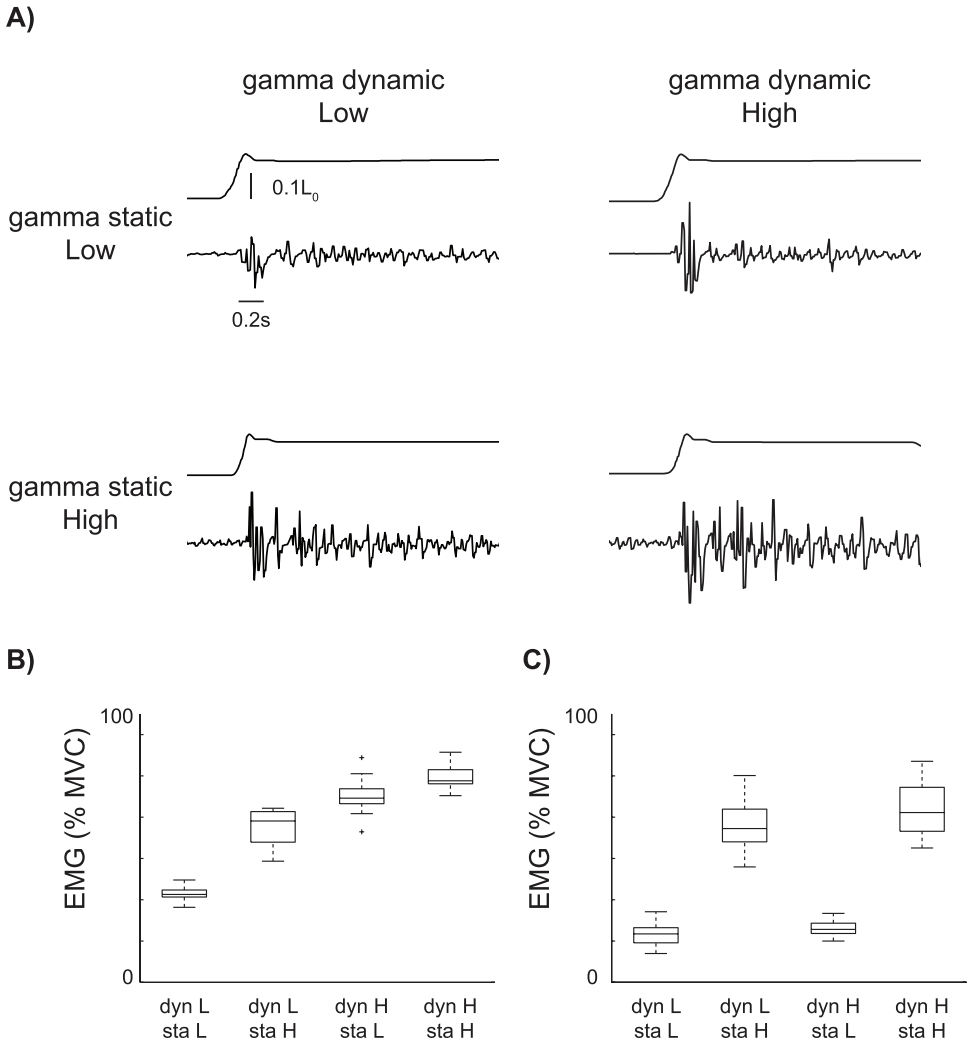

Figure 4. Emulated EMG responses when the cadaver finger was externally rotated, with 4 combinations of gamma dynamic and static. (A) Representative emulated EMG responses to a ramp-and-hold muscle stretch comprising of a burst and subsequent tonic components. (B) Across 15 repetitions, the emulated EMG traces showed variability due to the synaptic noise implemented in our system. Statistics show that EMG Bursts were affected by both gamma dynamic and static, but primarily gamma dynamic; the relative contributions of gamma dynamic and static were clearly disambiguated from EMG tonic responses.

and returned to the original angle after ~200 ms. This verifies that the chosen components from human sensorimotor system suffice to recover the original joint angle after a perturbation.

Our last experiment was to infer gamma activity during human experiments [45] using a neuromorphic reflex loop on a cadaver finger. We constructed three boundary cases to provide insights for inference (figure 7). Case 1: no static gamma, the spiking pattern has no static components. Case 2: no dynamic gamma, the spiking pattern has no break in the shortening period. Case 3: both velocity response and position response are present. From the comparison between human data and emulated results, it can be inferred that both gamma static and gamma dynamic need to be moderately active (at least 10 Hz) to allow sensing of elongation of the muscle fiber, while not being excessively active so that the spindle responses are low or silent during shortening.

Discussion

Decades of studies on neurophysiology provide an abundance of models characterizing components of the motor nervous system. The informational characteristics of physiological components allows us to model them as functional structures that convert input signals to certain outputs. In particular, within a monosynaptic spinal loop illustrated in figure 1(A), passive extension of the joint will elicit a chain of physiological activities in: muscle, muscle spindle, spindle afferents, synapses, motoneurons, and contractile elements of muscle. The techniques of neuromorphic modeling and emulation allow us to focus only on the informational consequence of each component. Therefore it becomes possible to probe all of the signals and states of the system. Our long-term goal is to understand the interactions among physiological components for creating sensorimotor functions. We are also interested in how small-scale abnormality may develop into clinical symptoms over time.

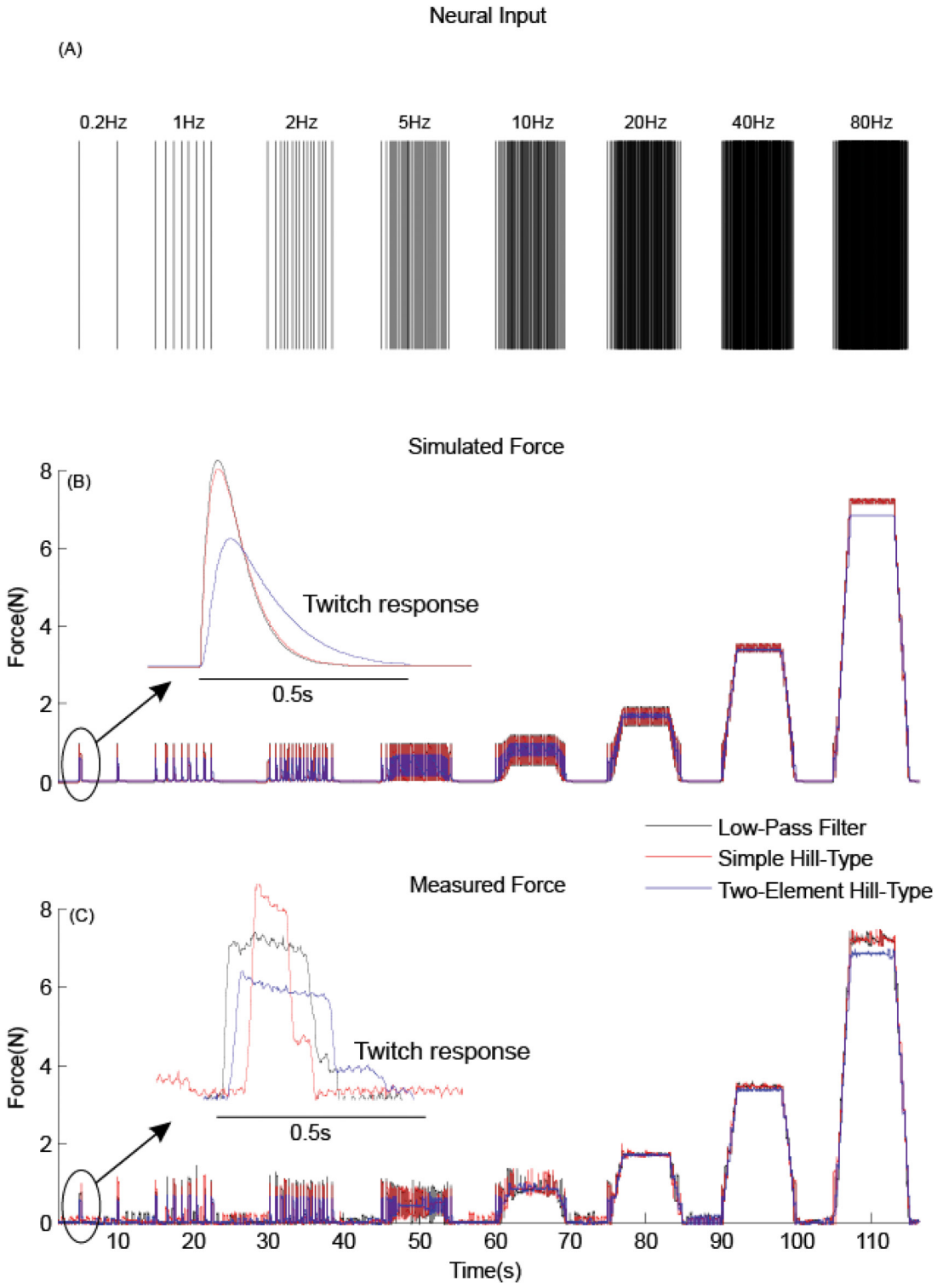

Figure 5. Software simulation and neuromorphic emulation of the low-pass filter, simple Hill-type and two element Hill-type muscle models in producing twitch response and unfused and fused tetanus responses: (A) action potential firing rate changed systematically from 0.2 to 80 Hz; (B) simulated forces from the three muscle models; (C) the measured forces of the neuromorphic system with the three muscle models.

It is important to highlight that this study presents a neuromorphic system that is meant to test the function of spinal circuits in the context of stretch reflexes. Thus we are not addressing the more general problem of cortico-spinal control of finger movements or forces. Rather, the work presented here is a critical first step towards creating neuromorphic systems to understand the nature and control of low-level neuromechanical function. Future studies will leverage this work to generate hypotheses about higher-level neural control of movement and force.

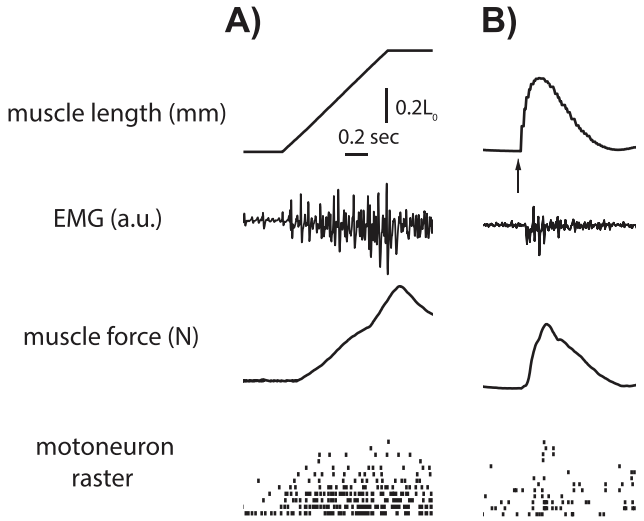

Figure 6. The emergent behavior with multi-scale information, when the robotic finger with hardware-in-the-loop was perturbed by a second robot (Phantom Desktop). Both gamma-dynamic and gamma-static drives were set to 80 Hz to provide moderate fusimotor activity. (A) Perturbation using a tonic force. The emulated force and EMG in the stretched muscle increased due to higher firing rates in the motoneuron pool. (B) Perturbation using a 4.0 N, 20 ms force pulse, the robotic joint was displaced by ~30° and returned to the original angle after ~200 ms. In the motoneuron raster panels, 2 neurons from each of the 6 motor unit pools (12 motoneurons) are shown. Due to the added motor noise, even the 2 neurons from the same motor unit pool did not show identical spike trains. This verifies that the chosen components from human sensorimotor system suffice to stabilize the joint.

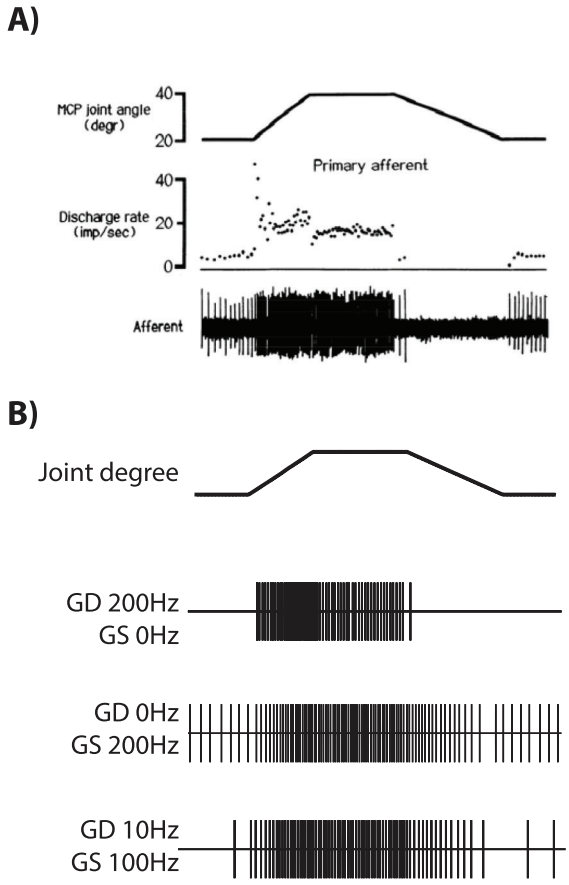

Figure 7. Inferring the gamma activity during human experiment using neuromorphic reflex loop on a cadaver finger. (A) Activity of a muscle spindle recorded from human [45], reproduced with permission. (B) Emulation Case 1: no static gamma, the spiking pattern has no static components. Case 2: no dynamic gamma, the spiking pattern has no break in the shortening period. Case 3: a mixed condition with both gamma dynamic and static activity, which shows both velocity response and position response.

Advantage of neuromorphic modeling

The importance of monosynaptic stretch reflex emulation for understanding the neural control of movement has not only been acknowledged in concept [38], but it also has been attempted several decades ago using analog circuits and mechanically simulated muscles [39]. In comparison to previous attempts, one technical advantage of our design is the neuromorphic modeling that enables emulation of spiking neurons. When both muscle drive and muscle spindle afferents are driven by spiking interfaces, it allows for future studies of long-term adaptation under the influence of spike-timing-dependent-plasticity (STDP), as well as the effect of medical intervention or disease that affects the membrane properties of neurons.

The current system did not include a cerebro-spinal component that is potentially crucial for the neural control of human hands. Nevertheless, due to the concurrent FPGA architecture it is straightforward to mount a supraspinal emulation on top of the existing system, without compromising its real-time performance. We have previously shown the utility of using a neuromorphic cerebro-spinal emulation to study the role of long-latency reflex in childhood dystonia [40].

Our system can be implemented on general-purpose neuromorphic platforms such as the Neural Engineering Framework [41], SPiNNaker [42], and others. The potential benefit includes accelerating spike-based algorithms using our high-speed spiking neural simulator in the loop, 'native' communication when stimulating live tissues without hand-designing the neural circuitry in hardware, and using spiking representation as an efficient coding strategy for system status.

Spindle responses

Figure 7(A) shows an initial burst in spindle firing rate which has also been documented in rats [43]. The physiological underpinning for the initial burst is probably due to stiction responses in presence of high gamma dynamic input, which is not incorporated in the original spindle model. In our previous work [15], we demonstrated that our emulation could produce such initial bursts, but similar firing rate comparisons were not available in this study due to restricted bandwidth in closed-loop emulations.

Cadaveric specimens

Figure 1(A) shows how it is critically important to validate such systems using actual cadaver fingers. From a purely mechanical standpoint, the tendon excursions that determine the muscle fiber length and velocity are neither assumed nor

approximated. They are the actual values seen in an anatomical system. Therefore, we can be assured that the mechanical input to the spindle afferent system is not only realistic, but also real. Moreover, the use of neuromorphic hardware to drive the tendons of cadaveric fingers is a novel and useful intermediate step between pure numerical simulations and system-wide microelectrode recordings in humans.

Muscle models

The selected muscle models represented different trade-offs between physiological realism and computational cost. The parameters of the first two (low-pass filter and simple Hill-type) models were tuned based on *in situ* studies of the cat soleus and frog gastrocnemius muscles. The parameters of the two-element Hill-type model were based on *in vivo* studies of the goat gastrocnemius muscle [44]. The choice of muscle model should be tailored to the specific need of future experiments. Differences between the measured forces and the software simulation seen in figure 5(C) are most likely explained by the limited bandwidth as the force did not imitate the high frequency oscillation of unfused tetanus response especially for neural firing rate above 10 Hz. Overall, it is within our interest to test and compare the different models in a repertoire of functional postural and movement.

Conclusions

This work is the first presentation of a methodology to build an electromechanical system that implements physiological principles of the sensorimotor control of afferented muscles. The neuromorphic technology enables emulation of spiking neurons, and the interconnection among neurons follows experimentally identified circuitry. The methodology was validated by systematically adding complexity to the emulation and comparing the results with known experiments in neurophysiology. Using this methodology, we demonstrated that this simplified neuromorphic model of the sensorimotor systems suffices to produce realistic reflex behavior. Furthermore, it enables us to examine the effect of muscle properties on the closed-loop behavior by considering both the passive and active nature of muscle. In Part II of this work, we will show that it enables us to explore for the first time the effect of fusimotor drive on the reflex response. Nevertheless, these results are only a first step that justifies future work to produce more quantitative comparisons between neuromorphic and physiological recordings. Despite limitations and simplifications, our neuromorphic system provides a synthetic analysis approach that creates a unique research platform for understanding how spinal neurons and circuitry produce healthy and pathologic sensorimotor behavior.

Acknowledgments

This project was supported by National Natural Science Foundation of China (Grant No. 81501570) to CM Niu, and the Youth Eastern Scholar program at Shanghai Institutions of Higher Learning (Award No. QD2015007) to CM Niu. The authors are grateful for support from Fonds de Recherche du Québec- Nature et Technologies to K Jalaleddini, and the James S McDonnell Foundation to TD Sanger. Research reported in this publication was supported by the National Institute of Arthritis and Musculoskeletal and Skin Diseases of the National Institutes of Health under Awards Number R01 AR050520 and R01 AR052345 to FJ Valero-Cuevas, and the National Institute of Neurologic Disorders and Stroke award R01 NS069214 to TD Sanger. The contents of this endeavor are solely the responsibility of the authors and do not necessarily represent the official views of the National Institutes of Health.

The authors thank Dr Gerald Loeb for insightful comments on the manuscript and assistance with design and analysis of experiments. The authors thank Dr Emily Lawrence, Dr Nina R Lightdale-Miric, Victor Barradas and Christoff Sulzenbacher for their help in preparation of the cadaveric specimen and for their help during data collection.

Author contribution statement

CMN prepared the neuromorphic platform with essential technical developments and designed and carried out the experiments. CMN and KJ conducted the analysis. WS and JR contributed to the development and analysis. JFV and TDS conceived and supervised the experiments and technical development and led preparation of the manuscript.

References

[1] Schieber M H 2011 Dissociating motor cortex from the motor *J. Physiol.* **589** 5613–24
[2] Lemon R N 1993 The G L Brown prize lecture. Cortical control of the primate hand *Exp. Physiol.* **78** 263–301
[3] Lemon R 2004 Cortico-motoneuronal system and dexterous finger movements *J. Neurophysiol.* **92** 3601
[4] McCulloch W S and Pitts W 1943 A logical calculus of the ideas immanent in nervous activity *Bull. Math. Biophys.* **5** 115–33
[5] Hodgkin A L and Huxley A F 1952 A quantitative description of membrane current and its application to conduction and excitation in nerve *J. Physiol.* **117** 500–544
[6] Rosenblatt F 1958 The perceptron: a probabilistic model for information storage and organization in the brain *Psychol. Rev.* **65** 386–408
[7] Mead C 1989 *Analog VLSI and Neural Systems* (Boston, MA: Addison-Wesley)
[8] Serrano-Gotarredona R *et al* 2009 CAVIAR: a 45k neuron, 5M synapse, 12G connects/s AER hardware sensory-processing-learning-actuating system for high-speed visual object recognition and tracking *IEEE Trans. Neural Netw.* **20** 1417–38
[9] Indiveri G *et al* 2011 Neuromorphic silicon neuron circuits *Front. Neurosci.* **5** 73
[10] Neftci E, Das S, Pedroni B and Kreutz-Delgado K 2013 Event-driven contrastive divergence for spiking neuromorphic systems *Front. Neurosci.*
[11] Chicca E, Badoni D, Dante V, D'Andreagiovanni M, Salina G, Carota L, Fusi S and Del Giudice P 2003 A VLSI recurrent network of integrate-and-fire neurons connected by plastic synapses with long-term memory *IEEE Trans. Neural Netw.* **14** 1297–307

[12] Lichtsteiner P, Posch C and Delbruck T 2008 A 128 × 128 120 dB 15 μs latency asynchronous temporal contrast vision sensor *IEEE J. Solid-State Circuits* **43** 566–576
[13] Eliasmith C, Stewart T C, Choo X, Bekolay T, DeWolf T, Tang Y, Tang C and Rasmussen D 2012 A large-scale model of the functioning brain *Science* **338** 1202–5
[14] Elias L A, Watanabe R N and Kohn A F 2014 Spinal mechanisms may provide a combination of intermittent and continuous control of human posture: predictions from a biologically based neuromusculoskeletal model *PLoS Comput. Biol.* **10** e1003944
[15] Niu C M, Nandyala S K and Sanger T D 2014 Emulated muscle spindle and spiking afferents validates VLSI neuromorphic hardware as a testbed for sensorimotor function and disease *Front. Comput. Neurosci.* **8** 141
[16] Izhikevich E M 2003 Simple model of spiking neurons *IEEE Trans. Neural Netw.* **14** 1569–72
[17] Mileusnic M P, Brown I E, Lan N and Loeb G E 2006 Mathematical models of proprioceptors. I. Control and transduction in the muscle spindle *J. Neurophysiol.* **96** 1772–88
[18] Niu C M, Nandyala S, Sohn W J and Sanger T D 2012 Multi-scale hyper-time hardware emulation of human motor nervous system based on spiking neurons using FPGA *Adv. Neural Inf. Process. Syst.* **25** 37–45
[19] McMahon T A 1984 *Muscles, Reflexes, and Locomotion* (Princeton, NJ: Princeton University Press)
[20] Henneman E 1957 Relation between size of neurons and their susceptibility to discharge *Science* **126** 1345–7
[21] Glowatzki E and Fuchs P A 2002 Transmitter release at the hair cell ribbon synapse *Nat. Neurosci.* **5** 147–54
[22] Mannard A and Stein R B 1973 Determination of the frequency response of isometric soleus muscle in the cat using random nerve stimulation *J. Physiol.* **229** 275–96
[23] Bobet J and Stein R B 1998 A simple model of force generation by skeletal muscle during dynamic isometric contractions *IEEE Trans. Biomed. Eng.* **45** 1010–6
[24] Brown I E, Scott S H and Loeb G E 1996 Mechanics of feline soleus: II. Design and validation of a mathematical model *J. Muscle Res. Cell Motil.* **17** 221–33
[25] Zajac F E 1989 Muscle and tendon: properties, models, scaling, and application to biomechanics and motor control *Crit. Rev. Biomed. Eng.* **17** 359–411
[26] Cheng E J, Brown I E and Loeb G E 2000 Virtual muscle: a computational approach to understanding the effects of muscle properties on motor control *J. Neurosci. Methods* **101** 117–30
[27] Hill A 1938 The heat of shortening and the dynamic constants of muscle *Proc. R. Soc.* B **126** 136–95
[28] Shadmehr R and Wise S P 2005 A mathematical muscle model *Supplementary Documents for 'Computational Neurobiology of Reaching and Pointing'* (Cambridge, MA: MIT Press) pp 1–18
[29] Wakeling J M, Lee S S M, Arnold A S, de Boef Miara M and Biewener A A 2012 A muscle's force depends on the recruitment patterns of its fibers *Ann. Biomed. Eng.* **40** 1708–20
[30] De Luca C J and Hostage E C 2010 Relationship between firing rate and recruitment threshold of motoneurons in voluntary isometric contractions *J. Neurophysiol.* **104** 1034–46
[31] Fellous J M, Rudolph M, Destexhe A and Sejnowski T J 2003 Synaptic background noise controls the input/output characteristics of single cells in an *in vitro* model of *in vivo* activity *Neuroscience* **122** 811–29
[32] George M and Alfke P 2001 Linear feedback shift registers in virtex devices *Xilinx Appl. Note* 1–5
[33] Valero-Cuevas F J, Towles J D and Hentz V R 2000 Quantification of fingertip force reduction in the forefinger following simulated paralysis of extensor and intrinsic muscles *J. Biomech.* **33** 1601–9
[34] Fuglevand A J, Winter D A and Patla A E 1993 Models of recruitment and rate coding organization in motor-unit pools *J. Neurophysiol.* **70** 2470–88
[35] Matthews P B C 1972 *Mammalian Muscle Receptors and Their Central Actions* (London: Hodder Arnold)
[36] Valero-Cuevas F J, Hoffmann H, Kurse M U, Kutch J J and Theodorou E A 2009 Computational models for neuromuscular function *IEEE Rev. Biomed. Eng.* **2** 110–35
[37] Biewener A A, Wakeling J M, Lee S S and Arnold A S 2014 Validation of Hill-type muscle models in relation to neuromuscular recruitment and force-velocity properties: predicting patterns of *in vivo* muscle force *Integr. Comp. Biol.*
[38] Smith K A and Littman M 1993 Endpoint position control using biological concepts *Proc. of the 1993 Int. Symp. on Intelligent Control (Chicago, Illinois, USA: IEEE)* pp 255–60
[39] Littman M G, Liker M, Stubbeman W, Russakow J, McGee C, Gelfand J and Call B J 1989 Electromechanical analogs of human reflexes *Ann. New York Acad. Sci.* **563** 184–93
[40] Sohn W J, Niu C M and Sanger T D 2015 Increased long-latency reflex activity as a sufficient explanation for childhood hypertonic dystonia: a neuromorphic emulation study *J. Neural Eng.* **12** 36010
[41] Eliasmith C 2013 *How to Build a Brain: a Neural Architecture for Biological Cognition* (Oxford: Oxford University Press)
[42] Furber S B, Galluppi F, Temple S and Plana L A 2014 The SpiNNaker project *Proc. IEEE* **102** 652–65
[43] Haftel V K 2004 Movement reduces the dynamic response of muscle spindle afferents and motoneuron synaptic potentials in rat *J. Neurophysiol.* **91** 2164–71
[44] Lee S S M, Arnold A S, de Boef Miara M, Biewener A A and Wakeling J M 2013 Accuracy of gastrocnemius muscles forces in walking and running goats predicted by one-element and two-element Hill-type models *J. Biomech.* **46** 2288–95
[45] Edin B B and Vallbo A B 1990 Dynamic response of human muscle spindle afferents to stretch *J. Neurophysiol.* **63** 1297–306